

We are IntechOpen, the world's leading publisher of Open Access books Built by scientists, for scientists

6,900

Open access books available

186,000

International authors and editors

200M

Downloads

Our authors are among the

154

Countries delivered to

TOP 1%

most cited scientists

12.2%

Contributors from top 500 universities



WEB OF SCIENCE™

Selection of our books indexed in the Book Citation Index
in Web of Science™ Core Collection (BKCI)

Interested in publishing with us?
Contact book.department@intechopen.com

Numbers displayed above are based on latest data collected.
For more information visit www.intechopen.com



Syntheses and Applications of Titanium Compound Nanofiber Thin Films

Mitsunori Yada

Additional information is available at the end of the chapter

<http://dx.doi.org/10.5772/64072>

Abstract

Syntheses, characteristics, wettability, and antibacterial activity of a titanium phosphate nanobelt thin film and titanate nanofiber thin films formed on titanium plates are presented in this chapter.

Keywords: titanium phosphate, sodium titanate, wettability, antibacterial activity, thin film

1. Introduction

Vigorous efforts have been made in recent years to control the structure and morphology of ceramic nanoparticles. The formation of peculiar nanostructures and morphologies can expose a specific crystal surface or cause a high specific surface area or characteristic pore diameter distribution, which can result in the manifestation of various peculiar physical and chemical properties. Vigorous efforts have been made to form the thin film comprised of nanoparticles, which should help peculiar physical and chemical properties of nanoparticles manifest more efficiently. The dip-coating, spin-coating, and electrophoretic deposition methods are commonly used to form the thin film, but they tend to cause nanoparticles to be randomly deposited on substrates, and the adhesion between the particles and substrate is often not good. An alternative method to form the thin film involves forming a nanostructured metal compound thin film on a metal surface where the metal itself is used as the raw material. Because the metal compound grows crystals directly on the metal surface in the nanostructured metal compound thin film/metal composites, superior adhesion between the metal and the thin film can be expected. In addition, the particle arrangement can be controlled by aligning the crystal

orientations of the particles to some degree. The superior electrical conductivity and mechanical properties of the metal and the peculiar physical and chemical properties of the nanostructured metal compound thin film can potentially provide a superior functional material that combines all such properties. Vigorous research efforts have been made on this aspect, particularly with regard to the synthesis of a nanostructured titanium compound thin film/titanium composite. This is because titanium compounds such as titanium dioxide and titanate feature superior characteristics for a broad range of applications, e.g., photocatalysts [1], dye-sensitized solar cells [2], lithium-ion batteries [3, 4], and biomaterials [5, 6]. Titanium dioxide and titanate are also extremely attractive because they are available at relatively low prices and are safe materials with no toxicity. Titanium dioxide and titanate have reportedly been used in such syntheses as the formation of a titanium dioxide nanotube thin film on a titanium metal surface with an electrochemical method (anodic oxidation of titanium metal) [6, 7], the formation of nanostructured titanate (nanotube, nanofiber, nanosheet, etc.) thin films on titanium metal surfaces by the reaction of titanium metal in an alkaline aqueous solution, and their conversions into nanostructured titanium dioxide thin film [5, 8–11]. For example, known applications of composites that utilize the superior electrical conductivity of titanium include electrode materials of dye-sensitized solar cells [12], lithium-ion batteries [13], and sodium-ion batteries [14]. Superior electrical conductivity can be secured by using titanium dioxide or titanate with one-dimensional morphologies, such as nanorods, nanotubes, or nanofibers, while electrodes can be prepared without using binders or conducting agents. Applied research on field emission materials [15] and electrochromic materials [16] of composites is also underway. On the other hand, biomaterials are a known application that utilizes the superior mechanical properties and safety of titanium metal. Titanium and titanium alloys are used as artificial joints based on their mechanical properties and safety inside the living body. Using composites adds osteoconductivity derived from titanium dioxide or titanate and antibacterial properties to titanium and titanium alloys, which facilitates the safe adhesion of bones and artificial joints in a short period of time [5, 6]. Antibacterial biomaterials are also desirable for medical sites; infections occur in 1–2% of artificial joint replacement surgeries and are a major problem [17, 18]. The present chapter evaluated the synthesis and antibacterial properties of titanate nanofiber thin film/titanium metal composites as an example application for biomaterials [10]. Various crystal structures such as $\text{Ti}(\text{HPO}_4)_2 \cdot \text{H}_2\text{O}$ and $\text{Ti}(\text{H}_2\text{PO}_4)\text{PO}_4 \cdot 2\text{H}_2\text{O}$ are known to exist with titanium phosphate. Morphology controls to shape nanotubes [19], nanofibers [20], elongated hexagonal nanoplates [21], and so on are also being developed. Applications of titanium phosphate include not just fundamental research on topics such as ion exchange and intercalation reactions but also catalysts [22], selective absorbents for toxic substances (e.g., Pb^{2+} , Cd^{2+}) [23, 24], the support and release of drugs [25], sodium batteries [26], and solar cells [27]. However, examples of reports on such efforts are primarily about particles, and there have not been many examples of studies on thin films. In particular, there are only three reports on the synthesis of titanium phosphate thin film on the surface of titanium, including the research of the present author. Lu et al. [28] immersed titanium in a phosphoric acid aqueous solution and induced a hydrothermal reaction at 250°C , while Park et al. [29] also immersed titanium in a phosphoric acid aqueous solution and induced a hydrothermal reaction at 180°C to form $\text{Ti}_2\text{O}(\text{PO}_4)_2(\text{H}_2\text{O})_2$ nanorod thin films on the titanium surface. Park et al. [29] revealed that such a thin film has

superior osteoconductivity. The present author added to these prior studies by discovering that titanium phosphate featuring a variety of crystal structures and morphologies is generated on the surface of a titanium plate immersed in an aqueous solution of hydrogen peroxide and phosphoric acid to produce a hydrothermal reaction [30]. This book is focused on nanofibers; this chapter narrows the focus to the titanium phosphate nanobelt thin film/titanium metal composite by introducing the formation mechanism and wettability.

2. Synthesis and wettability of a titanium phosphate nanobelt thin film

A titanium plate (20 mm × 20 mm × 0.5 mm) was scoured by using an abrasive paper and then immersed in 10 mL of an aqueous solution of 2 mol/L hydrogen fluoride for 10 min at room temperature to remove the surface-oxidized phase. It was then repeatedly washed with distilled water. A synthesis experiment of titanium phosphate thin film was performed with the derived plate. This experimental manipulation was performed in order to obtain a homogeneous titanium surface. This manipulation changed the morphology of the surface from that shown in **Figure 1a** to that shown in **Figure 1b** with a homogeneous surface morphology derived for each experiment. This plate was immersed in a mixture comprising 9.2 mL of 30 wt% H₂O₂ solution and 0.5 g of 85 wt% H₃PO₄ solution and left to react for 24 h at 120°C. Depending on the synthesis conditions (e.g., the raw material ratio or reaction temperature), this reaction generates high pressure inside the reaction container due to the generated gas, particularly when the hydrothermal reaction takes place at 100°C or higher. A reactor vessel that can measure the internal gas pressure while a reaction occurs inside and that is equipped with a safety valve to release the gas when required is desired. The obtained product was repeatedly washed with distilled water after the reaction. Because titanium phosphate particles that were generated in the solution during reaction deposited on the upper surface (front face), it was not possible to accurately evaluate the morphology of the titanium phosphate thin film growing from the titanium plate. Thus, a detailed evaluation was performed on the lower surface (back face) on which particles did not deposit. A thin film formed evenly on the surface of the titanium plate, as shown in **Figure 2a**. The thin film is composed of nanobelts with approximate widths of 30–270 nm and lengths of a few microns or more formed on the surface of the titanium plate, as shown in **Figure 2b** and **c**. The TEM image (**Figure 2c**) confirmed that the particles constituting the thin film were nanobelts because they were thin one-dimensional in morphology. Diffraction peaks that were attributed to titanium metal and Ti₂O₃(H₂PO₄)₂·2H₂O were observed in the X-ray diffraction measurements (**Figure 3**). They revealed that the nanobelts were made of Ti₂O₃(H₂PO₄)₂·2H₂O. Korösi et al. [25] reported on rectangular Ti₂O₃(H₂PO₄)₂·2H₂O nanoparticles with dimensions of 15 ± 3 nm × 20–150 nm. The nanobelts observed during this experiment, however, had nanoparticles with significant growth in the long axis direction. The thin film thickness was about 8 μm at the reaction time of 24 h but this thin film thickness became broader and reached 20 μm when the reaction time was extended to 72 h. SEM image of the thin film cross-section at the reaction time of 72 h are shown in **Figure 2d**. A phase comprising nanobelts was observed from the top surface of the

thin film down to a depth of about 18 μm . On the side closer to the titanium plate of the thin film, however, a phase of about 2 μm that was relatively dense was observed.

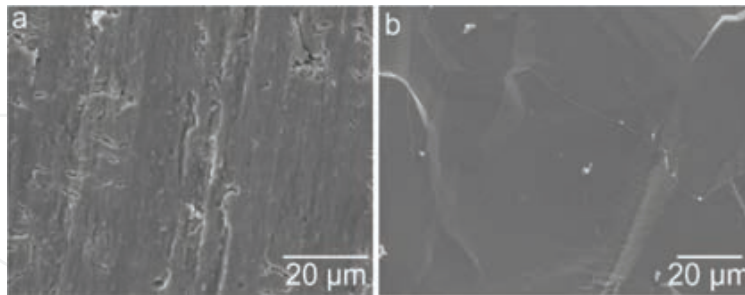


Figure 1. SEM images of the titanium plates before (a) and after (b) the HF treatment.

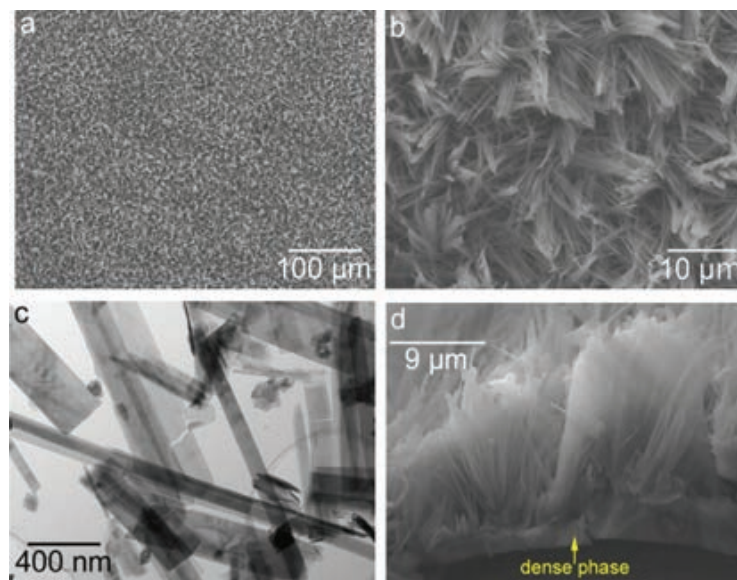


Figure 2. SEM images (a, b, and d) and a TEM image (c) of the titanium phosphate nanobelt thin films formed on titanium plates.

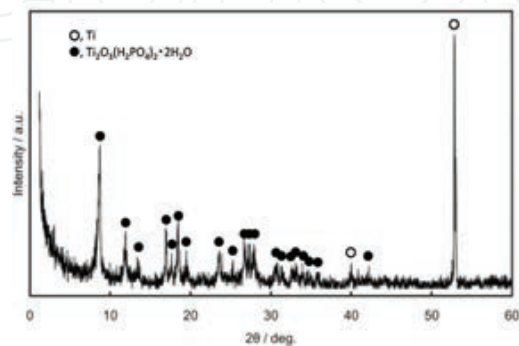


Figure 3. XRD pattern of the titanium phosphate nanobelt thin film.

The role of hydrogen peroxide was examined in order to consider the formation mechanism of nanobelts. This is because past studies that did not involve the use of hydrogen peroxide did not generate $\text{Ti}_2\text{O}_3(\text{H}_2\text{PO}_4)_2 \cdot 2\text{H}_2\text{O}$, as described earlier [28, 29]. In order to investigate the impact of hydrogen peroxide on the formation of the thin film, synthesis was performed with a fixed reaction temperature, reaction time, and phosphoric acid quantity of 120°C , 24 h, and 0.5 g, respectively, with varying quantities of hydrogen peroxide and water. When 9.2 mL of water was used for synthesis instead of hydrogen peroxide, the thin film did not form, and the formation of TiH_2 was observed in the XRD measurement. This confirmed that hydrogen peroxide plays an important role in the formation of the $\text{Ti}_2\text{O}_3(\text{H}_2\text{PO}_4)_2 \cdot 2\text{H}_2\text{O}$ nanobelt thin film. **Figure 4** shows a schematic representation of the formation mechanism for nanostructured titanium phosphate thin films based on the above results. Hydrogen peroxide has two primary roles. First, it acts as an oxidizer. Hydrogen peroxide acts as an oxidizer in acid solutions according to the following reaction formula:

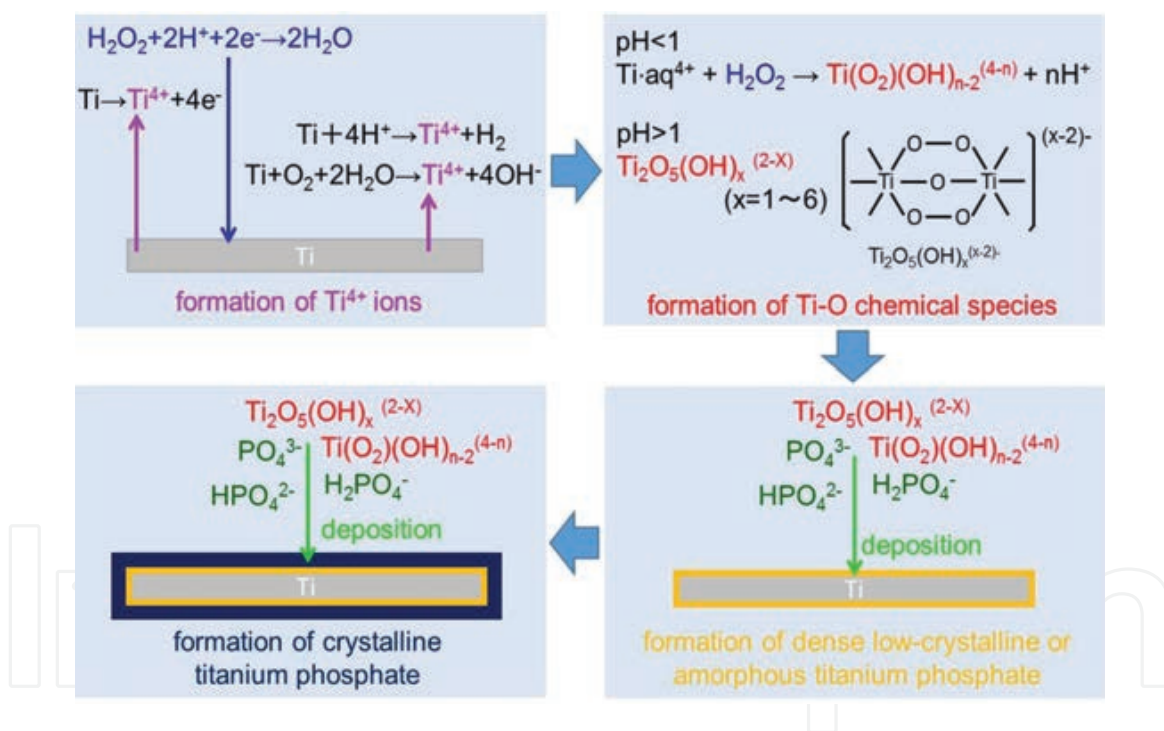
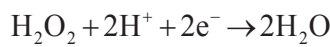
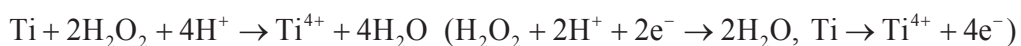


Figure 4. Schematic representation of the formation mechanism of the nanostructured titanium phosphate thin film formed on a titanium plate.

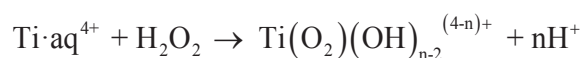
Therefore, hydrogen peroxide promotes the generation of Ti^{4+} from the titanium plate, as described by the following equation:



Although Ti^{4+} can be generated according to the following reaction formula by H^+ or dissolved oxygen in the aqueous solution, hydrogen peroxide has the greatest effect on promoting Ti^{4+} generation:



Ti^{4+} eluted from Ti into the reaction solution immediately starts to react with H_2O_2 . Ti^{4+} is known to react with hydrogen peroxide when $\text{pH} < 1$ [31].



Furthermore, binuclear complexes such as $\text{Ti}_2\text{O}_5(\text{OH})_x^{(2-x)}$ ($x = 1-6$) are known to be generated when $\text{pH} > 1$ [31]. These are referred to as peroxotitanic acid complexes and are indicated by a yellow color in the aqueous solution. The color of the solution after synthesis of the titanium phosphate nanobelt thin film was actually yellow, as shown in **Figure 5**, which indicates that a peroxotitanic acid complex was formed. Therefore, the second role of hydrogen peroxide is the formation of chemical species that contain Ti–O bonds. When such chemical species react with H_2PO_4^- ions, a relatively dense phase is formed first as an amorphous or low-crystalline titanium phosphate phase precipitates on the titanium plate. The nanobelt thin film forms next as high-crystalline $\text{Ti}_2\text{O}_3(\text{H}_2\text{PO}_4)_2 \cdot 2\text{H}_2\text{O}$, which is the most stable phase, grows on the surface of the dense phase. The formation of such a dense amorphous phase is important to link the titanium metal with $\text{Ti}_2\text{O}_3(\text{H}_2\text{PO}_4)_2 \cdot 2\text{H}_2\text{O}$, which has a completely different crystal structure. The phenomenon of a peculiar nanostructured thin film forming via the formation of a relatively dense phase on a metal surface has also been observed for the formation of sodium titanate thin films on titanium plate surfaces [9], which is described later. Synthesis using a mixture comprising 2.3 mL of hydrogen peroxide and 6.9 mL of water instead of 9.2 mL of hydrogen peroxide led to a flower-like aggregate of semispherical morphologies having a diameter of about a few tens of microns while the composition remained the same as $\text{Ti}_2\text{O}_3(\text{H}_2\text{PO}_4)_2 \cdot 2\text{H}_2\text{O}$. This means that a thin film comprising microflowers was generated (**Figure 6a**). Observation of the cross-section revealed that the thickness of the thin film was about 30 μm , and the microflower comprised particles with a nanoplate morphology about 400–700 nm wide and about 30–40 μm long growing in a radial pattern. A thin film of $\text{Ti}_2\text{O}_3(\text{H}_2\text{PO}_4)_2 \cdot 2\text{H}_2\text{O}$ having an intermediate morphology between the nanobelt thin film (**Figure 2b**) and microflower thin film (**Figure 6a**) was formed by using a mixture comprising 4.6 mL of hydrogen peroxide and 4.6 mL of water instead of 9.2 mL of hydrogen peroxide, as shown in **Figure 6b**. These results indicate the following formation process. The number of nuclei of $\text{Ti}_2\text{O}_3(\text{H}_2\text{PO}_4)_2 \cdot 2\text{H}_2\text{O}$ formed on the titanium plate decreased significantly once the amount of hydrogen peroxide in the reaction solution decreased. The microflower thin film

was believed to have been formed as a large number of $\text{Ti}_2\text{O}_3(\text{H}_2\text{PO}_4)_2 \cdot 2\text{H}_2\text{O}$ crystals slowly grew radially from these nuclei, which were just a few in number. Therefore, the morphology of the thin film can clearly be controlled in a variety of ways while the composition of $\text{Ti}_2\text{O}_3(\text{H}_2\text{PO}_4)_2 \cdot 2\text{H}_2\text{O}$ is maintained by controlling the synthesis conditions as described above.

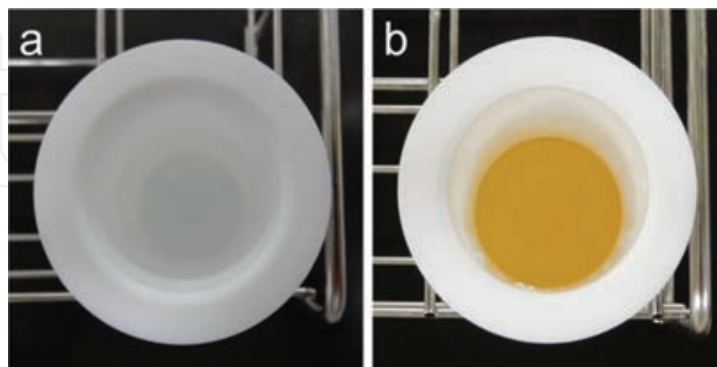


Figure 5. Digital camera images of the solutions before (a) and after (b) the reaction.

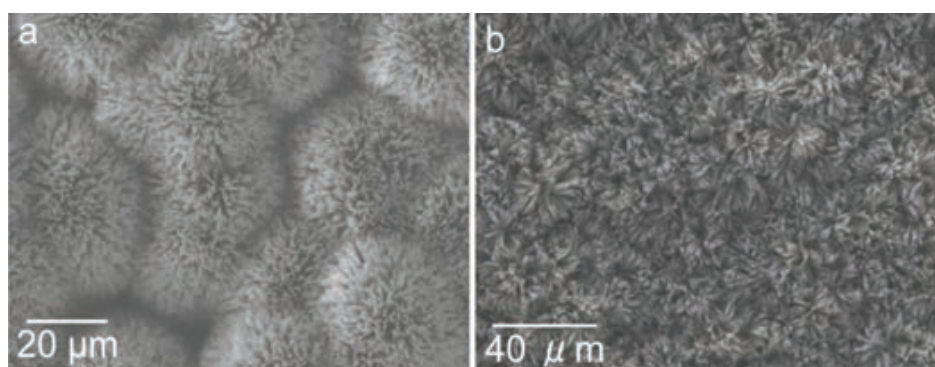


Figure 6. SEM images of $\text{Ti}_2\text{O}_3(\text{H}_2\text{PO}_4)_2 \cdot 2\text{H}_2\text{O}$ thin films formed on titanium plates.

Thin films with compositions other than $\text{Ti}_2\text{O}_3(\text{H}_2\text{PO}_4)_2 \cdot 2\text{H}_2\text{O}$ or of various morphologies other than nanobelts can be generated by controlling the raw material ratios and reaction temperatures, although no detailed descriptions are provided here because this chapter is focused on nanobelts. For instance, a thin film composed of anatase-type titanium dioxide and about 2 μm thick, a few tens of nanometers wide, and about 2 μm long—similar to that reported by Wu et al. [32]—was generated when synthesis was performed with a reaction temperature of 120°C, 9.2 mL of 30 wt% H_2O_2 solution, 0 g of 85 wt% H_3PO_4 solution, and reaction time of 24 h. A thin film about 8 μm thick, which appears to have been composed of hexagonal $\text{Ti}(\text{HPO}_4)_2 \cdot \text{H}_2\text{O}$ nanoplates a few microns in size, was derived when synthesis was performed with a reaction temperature of 120°C, 9.2 mL of 30 wt% H_2O_2 solution, 5 g of 85 wt% H_3PO_4 solution, and reaction time of 24 h (**Figure 7a**). A 2- μm -thick thin film composed of low-crystalline $\text{Ti}_2\text{O}_3(\text{H}_2\text{PO}_4)_2 \cdot 2\text{H}_2\text{O}$ nanosheets about a few hundred nanometers to 2 μm in size was formed when synthesis was performed with a reaction temperature of 80°C, 9.2 mL of 30 wt% H_2O_2 solution, 0.5 g of 85 wt% H_3PO_4 solution, and reaction time of 24 h (**Figure 7b**). A

thin film about 20 μm thick composed of $\text{Ti}_2\text{O}(\text{PO}_4)_2\text{H}_2\text{O}$ nanorods about 80–200 nm in diameter and a dozen or so microns long was formed when synthesis was performed with a reaction temperature of 160°C, 9.2 mL of 30 wt% H_2O_2 solution, 0.5 g of 85 wt% H_3PO_4 solution, and reaction time of 24 h (Figure 7c).

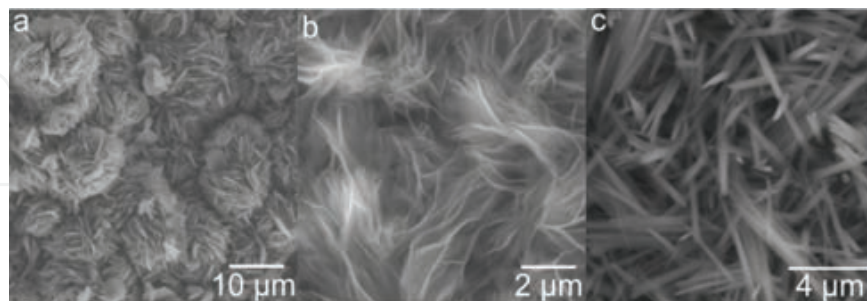


Figure 7. SEM images of the hexagonal $\text{Ti}(\text{HPO}_4)_2\cdot\text{H}_2\text{O}$ nanoplate thin film (a), the $\text{Ti}_2\text{O}_3(\text{H}_2\text{PO}_4)_2\cdot 2\text{H}_2\text{O}$ nanosheet thin film (b), and the $\text{Ti}_2\text{O}(\text{PO}_4)_2\cdot\text{H}_2\text{O}$ nanorod thin film (c).

The wettability of these thin films was investigated since titanium phosphate thin films having a diverse range of surface morphologies were derived, as described above. The wettability of a surface is generally determined by the surface energy and uneven structure of the surface [33]. In cases where the surface energy is high, the thin film tends to be hydrophilic; when the surface energy is low, it tends to be hydrophobic. Furthermore, the wettability is enhanced when an uneven structure is formed on a surface. When a water droplet was dropped on a synthesized titanium phosphate thin film, the droplet spread instantaneously, which indicates super-hydrophilicity. When the thin film was immersed in a 0.1 mol/L n-dodecyl decylamine hydrochloride solution of 2-propanol, on the other hand, the hydrophilicity decreased because the surface energy decreases when dodecylamine is adsorbed on the surface of titanium phosphate. The contact angle was 25° with the nanobelt thin film, 98° with the microflower thin film, 151° with the nanorod thin film, 151° with the nanoplate thin film, and 128° with the nanosheet thin film. Thus, the contact angle varies significantly depending on the composition and morphology of the thin film. Common features of test specimens with larger contact angles (nanorod thin film, nanoplate thin film and nanosheet thin film) were that the gap between protruding parts was narrow, and the spacing was uniform. With the nanobelt thin film, on the other hand, there were portions where the spacing between protruding parts was narrow and others where they were wide since the nanobelts were bent. The wider sections in such instances decreased the contact angle. Furthermore, the contact angle may have been reduced because there were portions on the microflower thin film where titanium phosphate microflowers were not generated and water was absorbed.

3. Synthesis and antibacterial activity of titanate nanofiber thin films

A titanium plate (20 mm × 20 mm × 2 mm) was immersed in 20 mL of a NaOH aqueous solution in a Teflon container; a hydrothermal reaction occurred at 160°C for 20 h. The derived product

was then washed repeatedly with water to produce a titanium plate covered by a sodium titanate nanofiber thin film on the surface, i.e., a sodium titanate nanofiber thin film/titanium metal composite. A digital camera photograph and a SEM image (**Figure 8a**) confirmed that nanofibers were formed uniformly on the surface of the titanium metal. SEM observation of the cross-section revealed that the thin film thickness was about 5 μm . Furthermore, the TEM images revealed that the nanofibers were a few tens to a hundred nanometers in width and a few microns in length (**Figure 8b**). The diffraction peaks attributed to titanate were observed in the X-ray diffraction pattern of the thin film. A Na:Ti:O molar ratio of 1:3.04:6.08 was determined from the EDS analysis of the thin film. This approximates the molar ratio for $\text{Na}_2\text{Ti}_6\text{O}_{13}$. Thus, the thin film was considered to be a $\text{Na}_2\text{Ti}_6\text{O}_{13}$ nanofiber thin film. The morphology of the sodium titanate thin film can be controlled according to the concentration and reaction temperature of the aqueous solution of NaOH. Using 1 mol/L NaOH aqueous solution instead of 4 mol/L NaOH aqueous solution resulted in the generation of a nanosheet thin film (**Figure 9a**) [10]. Using 10 mol/L NaOH aqueous solution resulted in the generation of a nanotube thin film (**Figure 9b**) [9]. Using 5 mol/L NaOH aqueous solution for a reaction at 60°C for 24 h resulted in the generation of a thin film with a porous network structure [5, 34].

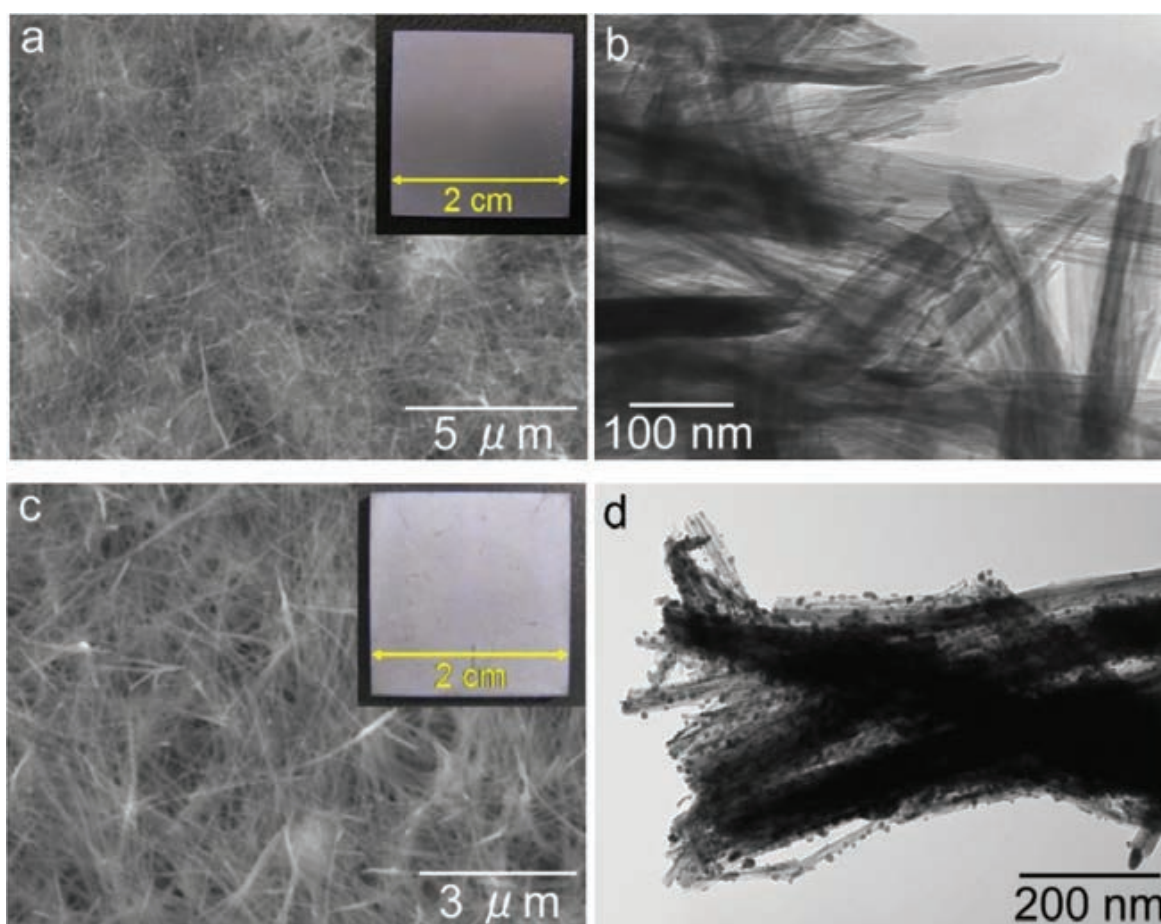


Figure 8. SEM images (a and c) and TEM images (b and d) of the sodium titanate nanofiber thin film (a and b) and the silver nanoparticles/silver titanate nanofiber thin film (c and d). Insets are photographs taken with a digital camera [10].

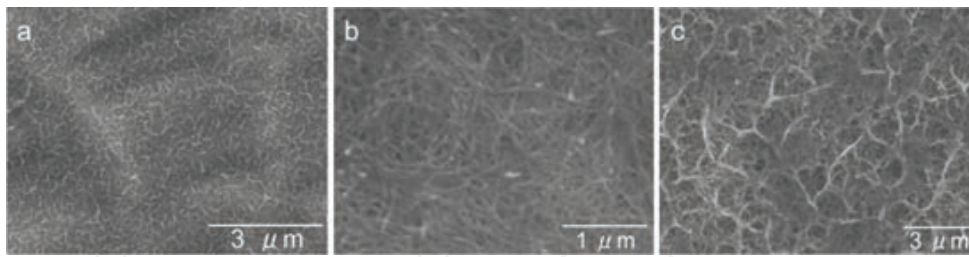


Figure 9. SEM images of the sodium titanate nanosheet thin film (a), the sodium titanate nanotube thin film (b) [34], and the sodium titanate thin film with a porous network structure (c) [34] formed on titanium plates.

The antibacterial activity of sodium titanate nanofiber thin film against methicillin-resistant staphylococcus aureus (MRSA) was investigated. MRSA is one of principal causative agents for nosocomial infection. Two types of tests were performed for the antibacterial test: the test specimen was irradiated and not irradiated with ultraviolet rays with the expectation of photocatalytic activity. Refer to the authors' previous paper for details on the methods used in the antibacterial tests [34]. The antibacterial activity value was used as an index for evaluation. The antibacterial activity value R is defined by the following equation; the antibacterial activity is considered to exist when $R \geq 2$.

$$R = \{\log(B/A) - \log(C/A)\} = \log(B/C)$$

Here, A is the viable bacterial count immediately after inoculation, B is the viable bacterial count of a blank test specimen 24 h later, and C is the viable bacterial count of the nanostructured titanate thin film 24 h later.

A high antibacterial activity value of 5.9 was recorded during the first round of antibacterial tests conducted under exposure to ultraviolet irradiation. Surprisingly, an extremely high antibacterial activity value of 5.8 was recorded even when a similar antibacterial test was conducted with no exposure to ultraviolet rays. This means that a high level of antibacterial activity was recorded for the nanofiber thin film during the first round of antibacterial tests regardless of whether or not the test specimen was exposed to ultraviolet rays. The antibacterial test was repeatedly performed using the same test specimen with and without (i.e., in a dark place) exposure to ultraviolet rays. Extremely high values of 7.7 and 6.6 were recorded for antibacterial activity during the second and third rounds of tests conducted under exposure to ultraviolet rays. Extremely low values of 1.0 and 0.3 were recorded for antibacterial activity during the second and third rounds of antibacterial tests conducted without exposure to ultraviolet rays. The above results revealed that (1) a high level of antibacterial activity manifested with the sodium titanate nanofiber thin film due to photocatalysis effects with exposure to ultraviolet rays and that (2) the sodium titanate nanofiber thin film has a high level of antibacterial activity immediately after synthesis, even when they are not exposed to any ultraviolet rays. Only the sodium titanate nanofiber thin film indicating a high level of antibacterial activity is extremely peculiar because the antibacterial activity of the sodium titanate nanosheet thin film and nanotube thin film described above were 2.1 [10] and 1.7 [34],

respectively. Treating such sodium titanate nanofiber thin film with a hydrochloric acid aqueous solution or heat-treating it at 600°C reduced the antibacterial activity value to 0.9 and 1.3, respectively, which eliminated the antibacterial activity. Because bacteria are known to have different properties that classify them as gram-positive or gram-negative depending on their structures, antibacterial tests regarding such individual bacteria types were also conducted. The antibacterial activity value of the sodium titanate nanofiber thin film was 5.5 against *Escherichia coli*, which is a gram-positive bacteria, and 4.7 against *Staphylococcus aureus*, which is a gram-negative bacteria. This reveals that sodium titanate nanofibers have a high level of antibacterial activity against bacteria of both structures. Because the reaction time was extended from 1 to 20 h, the formation of nanofibers was clarified according to the SEM images depicted in **Figure 10**. The intensities of the respective diffraction peaks were greater in the X-ray diffraction pattern, as shown in **Figure 11**. The antibacterial activity values of the thin films generated with reaction times of 1 and 5 h were 1.2 and 0.3, respectively, which indicates no antibacterial activity. The antibacterial activity value for the thin film generated with a reaction time of 12 h was 3.1; thus, the antibacterial activity manifested. The value was 6.5 for the thin film generated with a reaction time of 20 h; thus, a high level of antibacterial activity occurred. The above results indicate that the antibacterial activity increases with the growth of nanofibers and enhanced crystallinity. While it is not possible to offer any clear reason for such high levels of antibacterial activity at present, the following assumptions were made. All nanostructure morphologies (i.e., nanofiber, nanosheet, and nanotube) involve layering and rolling of titanate sheets, and the surface and the edge sections of titanate sheets can be considered separately because of their different chemical properties [35]. Nanofiber structures are characterized by having the highest proportion of the edge section to the overall area compared with other nanostructures. This may mean that the edges of titanate sheets become active sites and affect bacteria in some way, which manifests as a high level of antibacterial activity.

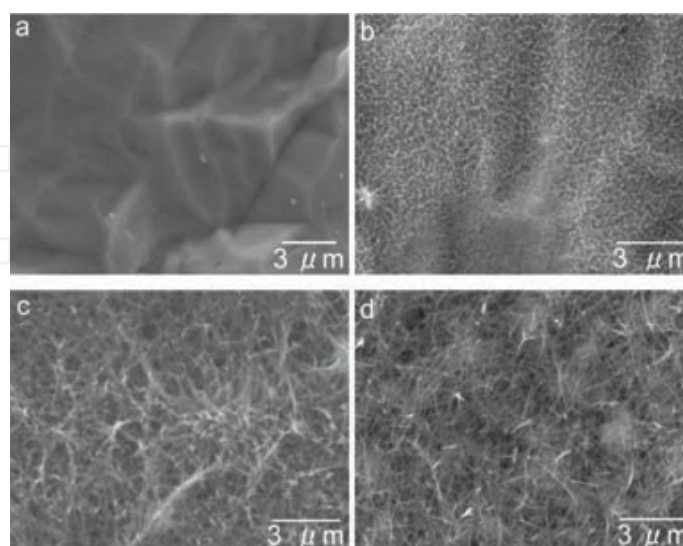


Figure 10. SEM images of sodium titanate nanofiber thin films synthesized following different reaction times; the titanium plate before the synthesis (a), and after 1 h (b), 5 h (c), and 12 h (d) reaction times [10].

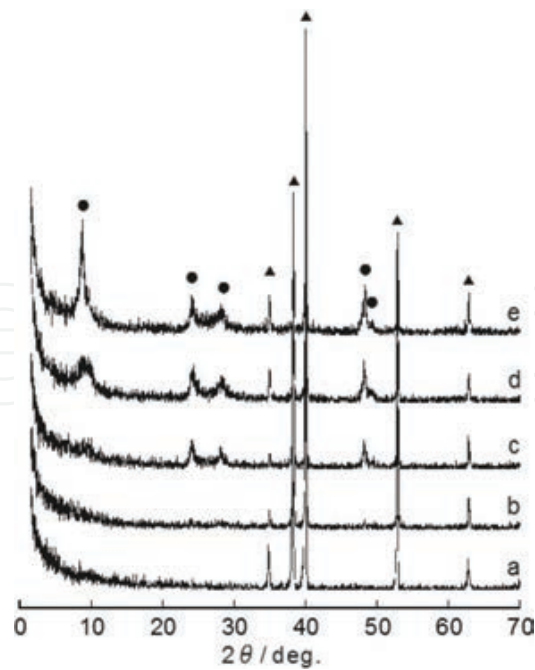


Figure 11. XRD patterns of sodium titanate nanofiber thin films following different reaction times; the titanium plate before the synthesis (a), and after 1 h (b), 5 h (c), 12 h (d), and 20 h (e) reaction times. Peak assignment: ●, sodium titanate; ▲, titanium [10].

Sodium titanate nanofiber thin film is considered to have poor practicality at the current point in time; while superior antibacterial activity was indicated during the first round of tests, the results from the second and subsequent rounds were not good, and there are many unknown aspects about the antibacterial mechanism. Silver, which is already being used in many studies on antibacterial materials, was therefore considered as an antibacterial component based on three considerations: (1) the superior antibacterial activity, (2) some degree of safety for living organisms, and (3) the relative lack of reports regarding the manifestation of drug-resistant bacteria [36]. Sodium titanate is a cation exchanger with a layered structure and can support silver in the titanate by exchanging Na^+ in sodium titanate with Ag^+ . A composite treated with silver ion exchange was derived by immersing the sodium titanate nanofiber thin film/titanium metal composite generated with a reaction time of 20 h in 12 mL of a 0.05 mol/L silver acetate aqueous solution at 40°C for 3 h, which was then washed repeatedly with distilled water and dried in a cool and dark location. The thin film derived after the silver ion exchange process remained firmly attached to the titanium plate, as shown in the digital camera photographs and SEM images in **Figure 8c**. There were no changes in the morphology, which had dimensions on the scale of microns. The TEM images, however, revealed precipitation of nanoparticles with dimensions of a few nanometers to a few tens of nanometers on the surface of the nanofiber (**Figure 8d**). These particles were considered to be silver nanoparticles, but no diffraction peaks attributed to silver were observed in the X-ray diffraction pattern (**Figure 12**). This may have been due to the small amount of precipitation that occurred because of the small diameters of the silver nanoparticles. No sodium was detected from the thin film after the silver ion exchange process, but silver was detected when the EDS analysis was conducted. A silver-to-titanium molar ratio of 0.638 was detected; this is greater than the

sodium-to-titanium molar ratio of 0.329 before the silver ion exchange process. Such results of the EDS analysis correspond to the precipitation of silver particles on the surface of nanofiber when Na^+ in the sodium titanate nanofiber was exchanged with Ag^+ . The X-ray diffraction pattern after the silver ion exchange process indicates the disappearance of the diffraction peak of $2\theta = 8.78^\circ$, which was caused by the layered structure observed with sodium titanate (Figure 12). Significant changes in the position and strength of the diffraction peaks at $2\theta \geq 15^\circ$ owing to the crystal structure of titanate were observed compared to before the silver ion exchange process (Figure 12). Such results indicate that the crystal structure of titanate changed from a two-dimensional layered structure to a three-dimensional crystal structure. The above results reveal that silver nanoparticles and silver titanate nanofiber thin film are generated by the silver ion exchange process of the sodium titanate nanofiber thin film. Such precipitation of silver nanoparticles on the surface of titanate and change in crystal structure caused by the silver ion exchange process have also been observed with the sodium titanate nanotube thin film and the sodium titanate thin film with a porous network structure [34]. This suggests that these are reaction behaviors common to layered titanates.

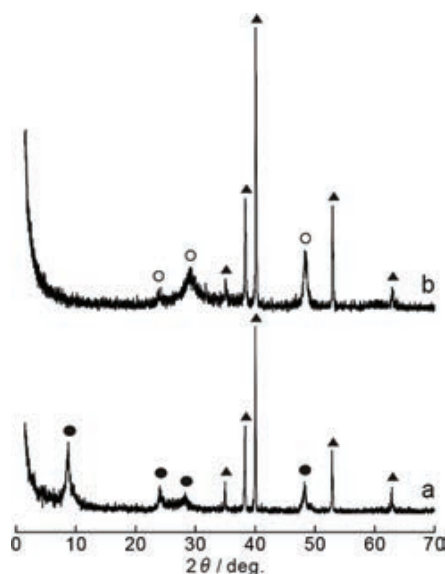


Figure 12. XRD patterns of the thin film before (a) and after (b) the silver ion exchange treatment. Peak assignment: ●, sodium titanate; ▲, titanium; ○, silver titanate [10].

The antibacterial activity value of the silver nanoparticles/silver titanate nanofiber thin film with respect to MRSA is 7.9, which is extremely high. This value is greater than the antibacterial activity value of 6.3 for a silver nanoparticles/silver titanate nanotube thin film or 7.8 for a silver nanoparticles/silver titanate thin film with a porous network structure [34]. The elution behavior of silver was investigated in fetal bovine serum (FBS) to simulate the environment of a living body because it was presumed to impact the antibacterial activity in a significant manner. Please refer to the authors' previous paper for details on the experimentation methods. Elution of 110 ppm was observed with silver nanoparticles/silver titanate nanofiber thin film, 94 ppm was observed with the silver nanoparticles/silver titanate nanotube thin film, and 68 ppm was observed with the silver particles/silver titanate thin film with a porous

network structure on the first day. The greatest amount of silver was clearly eluted by silver nanoparticles/silver titanate nanofiber thin film with the highest level of antibacterial activity. The orders of antibacterial activity and elution quantity for silver did not match completely. Therefore, antibacterial activity cannot be explained solely by the elution amount of silver. Although a clear examination is not possible at the present point in time, the surface morphology of the thin film is considered to be somehow related to the antibacterial activity. Chronologically, the amount of silver elution was 110 ppm on the first day, decreased to 77 ppm by the second day, and gradually decreased with subsequent days to 20 ppm by the tenth day. The elution of silver from silver nanoparticles and from silver titanate nanofiber due to the ion exchange reaction were considered as sources of silver elution from the thin film. FBS is known to contain a large amount of proteins and cations that readily bond with Ag^+ , and the ion exchange reaction is known to be extremely rapid. This means that it is extremely likely that the large amount of silver elution on the first day was due to the silver elution from the ion exchange reaction of silver titanate nanofibers. The contribution to silver elution by the silver titanate nanofibers decreased with time; instead, the silver elution from silver nanoparticles increased in their place. The antibacterial activity can be expected to be sustained over a long period since the silver nanoparticles/silver titanate nanofiber thin film can continue to elute silver in this manner for over 10 days.

4. Conclusion

This chapter introduces the generation of titanium compounds with various nanostructures, including titanium phosphate nanobelts and titanate nanofibers on the surface of titanium metal plate, from the treatment of a titanium metal plate in aqueous solutions of various compositions. Because aqueous solutions of various compositions and concentrations and different reaction temperatures and times can be combined for chemical processes involving titanium metal, novel titanium compounds/titanium metal composites with various compositions and nanostructures are expected to be synthesized in the future. It is important to continue with applied research on developing composites that feature the characteristics of both nanostructured titanium compounds and titanium metal, as described in Section "Introduction." In this manner, characteristics that surpass those of the nanostructured titanium compound particles can be derived. Research is expected to continue with applications including biomaterials and electrode materials intended for dye-sensitized solar cells, lithium-ion batteries, and sodium-ion batteries.

Acknowledgements

This research was partially supported by KAKENHI (19750172, 25420732). The author gives special thanks to Dr. Yuko Inoue, Miss Ayako Sakamoto, Miss Misaki Maeda, and Mr. Tomohiro Morita for their supports.

Author details

Mitsunori Yada

Address all correspondence to: yada@cc.saga-u.ac.jp

Department of Chemistry and Applied Chemistry, Faculty of Science and Engineering, Saga University, Saga, Japan

References

- [1] Schneider J, Matsuoka M, Takeuchi M, Zhang J, Horiuchi Y, Anpo M, Bahnemann D W. Understanding TiO₂ photocatalysis: mechanisms and materials. *Chem Rev.* 2014;114:9919–9986.
- [2] Roose B, Pathak S, Steiner U. Doping of TiO₂ for sensitized solar cells. *Chem Soc Rev.* 2015;44:8326–8349.
- [3] Sandhya C P, John B, Gouri C. Lithium titanate as anode material for lithium-ion cells: a review. *Ionics.* 2014;20:601–620.
- [4] Song T, Paik U. TiO₂ as an active or supplemental material for lithium batteries. *J Mater Chem A.* 2016;4:14–31.
- [5] Kokubo T, Yamaguchi S. Bioactive Ti metal and its alloys prepared by chemical treatments: state-of-the-art and future trends. *Adv Eng Mater.* 2010;12:B579–B591.
- [6] Kulkarni M, Mazare A, Gongadze E, Perutkova Š, Kralj-Iglič V, Milošev I, Schmuki P, Iglič A, Mozetič M. Titanium nanostructures for biomedical applications. *Nanotechnology.* 2015;26:062002.
- [7] Roy P, Berger S, Schmuki P. TiO₂ nanotubes: synthesis and applications. *Angew Chem Int Ed.* 2011;50:2904–2939.
- [8] Peng X, Chen A. Large-scale synthesis and characterization of TiO₂-based nanostructures on Ti substrates. *Adv Funct Mater.* 2006;16:1335–1362.
- [9] Yada M, Inoue Y, Uota M, Torikai T, Watari T, Noda I, Hotokebuchi T. Plate, wire, mesh, microsphere, and microtube composed of sodium titanate nanotubes on a titanium metal template. *Langmuir.* 2007;23:2815–2823.
- [10] Yada M, Inoue Y, Noda I, Morita T, Torikai T, Watari T, Hotokebuchi T. Antibacterial properties of titanate nanofiber thin films formed on a titanium plate. *J Nanomater.* 2013:47685.

- [11] Inoue Y, Noda I, Torikai T, Watari T, Hotokebuchi T, Yada M. TiO₂ nanotube, nanowire, and rhomboid-shaped particle thin films fixed on a titanium metal plate. *J Solid State Chem.* 2010;183:57–64.
- [12] Wu W-Q, Rao H-S, Xu Y-F, Wang Y-F, Su C-Y, Kuang D-B. Hierarchical oriented anatase TiO₂ nanostructure arrays on flexible substrate for efficient dye-sensitized solar cells. *Sci Rep.* 2013;3:1892.
- [13] Shen L, Uchaker E, Zhang X, Cao G. Hydrogenated Li₄Ti₅O₁₂ nanowire arrays for high rate Lithium Ion batteries. *Adv Mater.* 2012;24:6502–6506.
- [14] Li H, Fei H, Liu X, Yang J, Wei M. In situ synthesis of Na₂Ti₇O₁₅ nanotubes on a Ti net substrate as a high performance anode for Na-ion batteries. *Chem Commun.* 2015;51:9298–9300.
- [15] Miyauchi M, Tokudome H, Toda Y, Kamiya T, Hosono H. Electron field emission from TiO₂ nanotube arrays synthesized by hydrothermal reaction. *Appl Phys Lett.* 2006;89:043114.
- [16] Ghicov A, Tsuchiya H, Hahn R, Macak J M, Muñoz A G, Schmuki P. TiO₂ nanotubes: H⁺ insertion and strong electrochromic effects. *Electrochem Commun.* 2006;8:528–532.
- [17] Jämsen E, Furnes O, Engesæter L B, Konttinen Y T, Odgaard A, Stefánsdóttir A, Lidgren L. Prevention of deep infection in joint replacement surgery. *Acta Orthopaedica.* 2010;81:660–666.
- [18] Rasouli M R, Restrepo C, Maltenfort M G, Purtill J J, Parvizi J. Risk factors for surgical site infection following total joint arthroplasty. *J Bone Joint Surg Am.* 2014;96:e158.
- [19] Yin Z, Sakamoto Y, Yu J, Sun S, Terasaki O, Xu R. Microemulsion-based synthesis of titanium phosphate nanotubes via amine extraction system. *J Am Chem Soc.* 2004;126:8882–8883.
- [20] Bortun A I, Khainakov S A, Bortun L N, Poojary D M, Rodriguez J, Garcia J R, Clearfield A. Synthesis and characterization of two novel fibrous titanium phosphates Ti₂O(PO₄)₂·2H₂O. *Chem Mater.* 1997;9:1805–1811.
- [21] Liu J, Wei X. Supercritical synthesis of layered elongated hexagonal titanium phosphate nanoplates. *RSC Adv.* 2015;5:7798–7802.
- [22] Liu J, Wei X, Yu Y, Song J, Wang X, Li A, Liu X-W, Deng W-Q. Uniform core-shell titanium phosphate nanospheres with orderly open nanopores: a highly active Brønsted acid catalyst. *Chem Commun.* 2010;46:1670–1672.
- [23] Jia K, Pan B, Zhang Q, Zhang W, Jiang P, Hong C, Pan B, Zhang Q. Adsorption of Pb²⁺, Zn²⁺, and Cd²⁺ from waters by amorphous titanium phosphate. *J Colloid Interface Sci.* 2008;318:160–166.

- [24] Wang X, Yang X, Cai J, Miao T, Li L, Li G, Deng D, Jiang L, Wang C. Novel flower-like titanium phosphate microstructures and their application in lead ion removal from drinking water. *J Mater Chem A*. 2014;2:6718–6722.
- [25] Korösi L, Papp S, Dékány I. A layered titanium phosphate $\text{Ti}_2\text{O}_3(\text{H}_2\text{PO}_4)_2 \cdot 2\text{H}_2\text{O}$ with rectangular morphology: synthesis, structure, and cysteamine intercalation. *Chem Mater*. 2010;22:4356–4363.
- [26] María J A, Candela V-A, Pedro L, José L T. Improving the electrochemical performance of titanium phosphate-based electrodes in sodium batteries by lithium substitution. *J Mater Chem A*. 2013;1:13963–13969.
- [27] Park K-H, Mondal S, Ghosh S, Das S, Bhaumik A. Enhanced efficiency in dye-sensitized solar cells based on mesoporous titanium phosphate photoanode. *Microporous Mesoporous Mater*. 2016;225:255–260.
- [28] Lu J-S. Corrosion of titanium in phosphoric acid at 250°C. *Trans Nonferrous Met Soc China*. 2009;19:552–556.
- [29] Park J-W, Jang J-H, Lee C S, Hanawa T. Osteoconductivity of hydrophilic microstructured titanium implants with phosphate ion chemistry. *Acta Biomater*. 2009;5:2311–2321.
- [30] Yada M, Inoue Y, Sakamoto A, Torikai T, Watari T. Synthesis and controllable wettability of micro- and nanostructured titanium phosphate thin films formed on titanium plates. *ACS Appl Mater Interfaces*. 2014;6:7695–7704.
- [31] Mühlebach J, Müller K, Schwarzenbach G. Peroxo complexes of titanium. *Inorg Chem*. 1970;11:2381–2390.
- [32] Wu J-M. Low-temperature preparation of titania nanorods through direct oxidation of titanium with hydrogen peroxide. *J Cryst Growth*. 2004;269:347–355.
- [33] Yan Y Y, Gao N, Barthlott W. Mimicking natural superhydrophobic surfaces and grasping the wetting process: a review on recent progress in preparing superhydrophobic surfaces. *Adv Colloid Interface Sci*. 2011;169:80–105.
- [34] Inoue Y, Uota M, Torikai T, Watari T, Noda I, Hotokebuchi T, Yada M. Antibacterial properties of nanostructured silver titanate thin films formed on a titanium plate. *J Biomed Mater Res Part A*. 2010;92:1171–1180.
- [35] Matsumoto Y, Ida S, Inoue T. Photodeposition of metal and metal oxide at the TiO_x nanosheet to observe the photocatalytic active site. *J Phys Chem C*. 2008;112:11614–11616.
- [36] Chernousova S, Epple M. Silver as antibacterial agent: ion, nanoparticle, and metal. *Angew Chem Int Ed*. 2013;52:1636–1653.